Dartmouth College
Dartmouth Digital Commons

Open Dartmouth: Faculty Open Access Articles

2-1-2000

Spatially Resolved Spectroscopy of Coma Cluster Early–Type Galaxies

D. Mehlert
Universitäts-Sternwarte München

R. P. Saglia
Universitäts-Sternwarte München

R. Bender
Universitäts-Sternwarte München

G. Wegner
Dartmouth College

Follow this and additional works at: https://digitalcommons.dartmouth.edu/facoa

Part of the Stars, Interstellar Medium and the Galaxy Commons

Spatially resolved spectroscopy of Coma cluster early–type galaxies

I. The database[*]

D. Mehlert[1,2,**,***,****], **R.P. Saglia**[1], **R. Bender**[1], **and G. Wegner**[3]

[1] Universitätssternwarte München, 81679 München, Germany
[2] Present address: Landessternwarte Heidelberg, 69117 Heidelberg, Germany
[3] Department of Physics and Astronomy, 6127 Wilder Laboratory, Dartmouth College, Hanover, NH 03755-3528, U.S.A.

Abstract. We present long slit spectra for a magnitude limited sample of 35 E and S0 galaxies of the Coma cluster. The high quality of the data allowed us to derive *spatially resolved* spectra for a substantial sample of Coma galaxies for the first time. From these spectra we obtained rotation curves, the velocity dispersion profiles and the H_3 and H_4 coefficients of the Hermite decomposition of the line of sight velocity distribution. Moreover, we derive the radial line index profiles of Mg, Fe and $H\beta$ line indices out to $R \approx 1r_{\rm e} - 3r_{\rm e}$ with high signal-to-noise ratio. We describe the galaxy sample, the observations and data reduction, and present the spectroscopic database. Ground-based photometry for a subsample of 8 galaxies is also presented.

The Coma cluster is one of the richest known clusters of galaxies, spanning about 4 decades in density. Hence it is the ideal place to study the structure of galaxies as a function of environmental density in order to constrain the theories of galaxy formation and evolution. Based on the spectroscopic database presented, we will discuss these issues in a series of future papers.

1. Introduction

This is the first of a series of papers aiming at investigating the stellar populations, the radial distribution and the dynamics of early-type galaxies as a function of the environmental density. Spanning about 4 decades in density, the Coma cluster is the ideal place to perform such a study.

We describe ground-based photometry performed to select the outer sample in Sect. 2. The whole spectroscopic sample and its selection properties are discussed in Sect. 3. The spectroscopic observations and data reduction are described in Sect. 4. The spectroscopic database is presented in Sect. 5 and the comparisons with the literature are discussed in Sect. 6. Conclusions are drawn in Sect. 7.

2. Photometric observations and data reduction

The most uniform CCD photometry of the inner square degree of the Coma cluster is provided by Jørgensen & Franx (1994, JF94). The sample Lucey et al. (1991) investigated, is not complete, while the observations of Andreon et al. (1996, 1997) have been performed partially in very bad seeing conditions.

No CCD photometry of similar quality and uniformity as the data of JF94 exists for the galaxies of the outer region of the Coma cluster. Since one special issue of this project is to investigate the structure of galaxies as a function of their environmental density, complementary photometry was needed in the outer regions of the Coma cluster. Therefore we selected the 20 galaxies brighter

than $b_{26.5} = 15.0$ mag and with projected distances larger than 40 arcmin from the cluster center from the (photographic) catalogue of Godwin et al. (1983, GMP83). For these galaxies we obtained Kron-Cousins R_c band CCD surface photometry at the 1.3 m telescope of the MDM observatory in March 1995. We used a Loral 2048×2048 chip with a scaling of $0.508''$ per pixel and observed the galaxies for 500 s with a PSF of $1.5 - 2''$. Sky subtraction, cosmic ray elimination via a $\kappa - \sigma$ clipping procedure and the removal of foreground stars were performed with MIDAS packages. Following Bender & Möllenhoff (1987, BM87) the surface brightness profile of the galaxies were obtained by fitting the isophotes with ellipses. Furthermore the deviations from ellipses were studied by means of Fourier series expansions (see BM87)[1]. The resulting fourth cosine coefficients a_4 indicate boxy (negative values) or disky isophotes (positive values). Based on surface brightness, ellipticity, the a_4 and a_6 profiles as well as visual inspection eight of the investigated objects were classified to be early-type galaxies. The results of the isophotal shape analysis of these 8 galaxies are shown in Fig. 1 and listed in Tables 5 to 12 in Appendix A.

Also based on surface brightness, ellipticity and a_4 profiles as well as visual inspection of the CCD frames we classified the remaining 11 late-type galaxies as follows. S0/Sa: GMP3273; Sa: GMP1900, GMP2544, GMP2987, GMP5006, GMP6523; Sb: GMP3837, GMP6339; SB0: GMP5886; SBa: GMP6265; SBb: GMP5437. The data of these galaxies will be presented and discussed in a separate paper.

In order to be comparable to the data from JF94 we derived the luminosity weighted mean of a_4

$$\langle a_4 \rangle := \frac{\int_{a_{\min}}^{a_{\max}} I \times a_4 \, \mathrm{d}a}{\int_{a_{\min}}^{a_{\max}} I \, \mathrm{d}a}; \quad (a - \text{the semi-major axis}) \quad (1)$$

for the 8 early-type galaxies of the observed sample. The integration is done from $a_{\min} = 1.5''$ to the maximum semi-major axis $a_{\max}$ at which a_4 could be determined (see Tables 5 to 12). $\langle a_4 \rangle$ as well as the ellipticity at r_e of these 8 objects is listed in Table 1 (Nos. 28–35). According to BM87 the typical errors of a_4 and ϵ are 0.2% and 0.005, respectively.

For 5 of the 8 early-type galaxies in the outer sample HST V band surface photometry is available (Principal Investigator: John Lucey; Proposal ID: 5997). Because our data were taken in non-photometric nights we used these HST images to determine the V band zero-point and calibrated our R-band frames applying a typical colour for elliptical galaxies $V - R_{KC} = 0.6$ mag (Poulain & Nieto 1994, PN94). The scatter in $V - R_{KC} = 0.07$ mag and dominates the error in the zero point, while the accuracy due to the HST photometry is about 0.01 mag (Holtzman

et al. 1995). For the remaining 3 galaxies (GMP0756, 1176, 1990) we computed the zero-point using the b magnitudes inside the 26.5 mag/arcsec^2 surface brightness isophote as given by GMP83, adopting their mean $b - r$ colours. Their r band magnitudes are approximately equal to the Johnson R. To convert this Johnson R in Kron-Cousins magnitudes we used the colour equations given by Fernie (1983): $(V - R)_J = 0.034(\pm 0.05) + 1.364(\pm 0.016) (V - R)_{KC}$. Since V is the same in both systems and $V - R_{KC} = 0.6$ mag from PN94, this yields to $R_{KC} = R_J + 0.25$ (± 0.06). The accuracy of the zero-point is limited by the error given by GMP83 to be δ mag = 0.15 mag. Total magnitudes m_T, half luminosity radii r_e and the surface brightness SB_e at r_e were derived using the algorithm of Saglia et al. (1997a), which optimally fits the (circularly averaged) surface brightness profiles as a sum of seeing convolved $r^{1/4}$ and exponential components and corrects for sky subtraction errors. Saglia et al. (1997b) showed that the systematic errors due to the extrapolation method, sky subtraction and seeing convolution for the total magnitudes $\delta m_T < 0.15$ mag and for the effective radius is $\delta r_e < 10\%$. On the other hand the deviations that are introduced by using circular apertures instead of elliptical ones are significantly smaller ($\delta m_T < 0.05$ mag for $\epsilon < 0.5$; see Saglia et al. 1997a).

Finally, the values of the total magnitude m_T and the surface brightness SB have been corrected for galactic extinction and K – correction has also been applied. We have used the B band galactic extinction determined by Burstein & Heiles (1984). For GMP 0144, GMP 5568 and GMP 5975 $A_B = 0.03$ mag and can be converted to the R band using $A_R = 0.58 A_B$ (Seaton 1979). For the remaining five galaxies the same extinction is assumed. The K-correction was provided by Rocca-Volmerange & Guiderdoni (1988, $K_R = 0.028$ mag). The surface brightness was also corrected for cosmological $(1 + z)^4$ dimming. Table 1 shows the derived photometric parameter R_{c_T}, $\langle SB_e \rangle$ and r_e for the 8 observed early-type Galaxies in the outer part of the Coma cluster (Nos. 28–35).

Five of the 8 early type galaxies identified here were already previously observed by Lucey et al. (1991, Letal91). For four objects (Nos. 28, 29, 33, 35) the differences from our derived magnitudes are lower than the systematic errors (0.15 mag) described above. Only for galaxy No. 34 (GMP 5568) the difference is larger (0.75 mag), but Letal91 state that their photometric parameters are poorly defined. Their derived effective radii tend to be smaller than the values derived in this paper, since Letal91 fitted the surface brightness profile only with an $r^{1/4}$ law, neglecting any exponential component. Nevertheless the mean difference of the quantity $\log r_e - 0.3 \langle SB_e \rangle$ (see Saglia et al. 1997b) is negligible (0.03) and showing a scatter of only 0.01. Hence there is no systematic zeropoint offset the two dataset.

---

[1] In fact all Fourier coefficients a_i and b_i derived by BM87 are normalized to the semi-major axis a. Instead of writing a_i/a and b_i/a we use the short form a_i and b_i throughout the text.
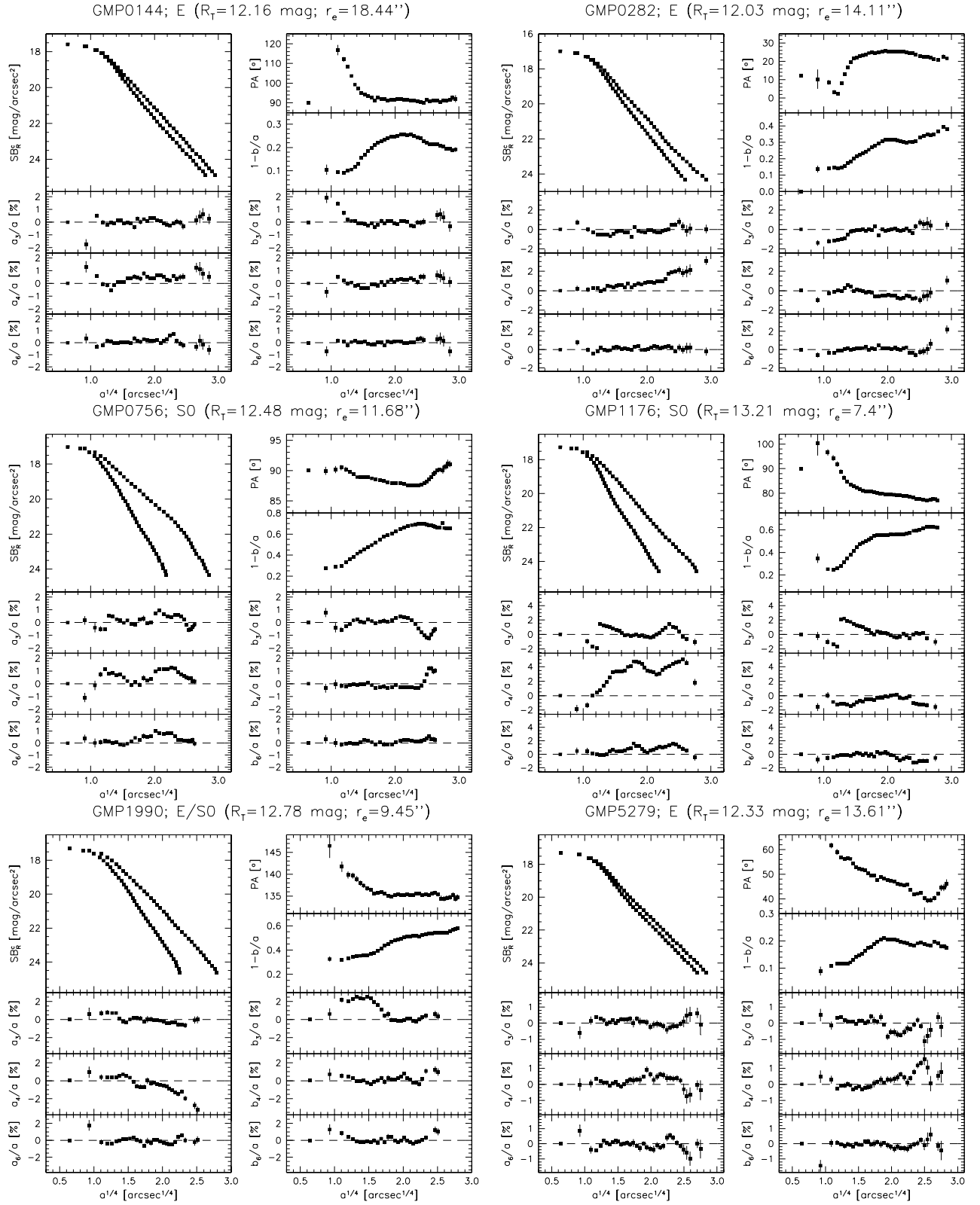
Fig. 1. The results of the isophote shape analysis of the CCD photometry of the 8 early type galaxies with $D > 40'$ and $b_{26.5} < 13$ mag. The plots to the left show (from top to bottom) the R-band surface brightness, the $a_3/a, a_4/a, a_6/a$ coefficients as a function of the 1/4 power of the semi-major axis distance a in arcsec. The surface brightness is shown along the major (upper profile) and the minor axis (lower profile). The plots to the right show (from top to bottom) the position angle, the ellipticity and the coefficients $b_3/a, b_4/a, b_6/a$

Fig. 1. continued

3. The galaxy sample

For the inner square degree of the Coma cluster we selected 27 early-type galaxies from the complete catalogue of JF94. E and S0 galaxies were selected separately accordingly to the following strategy:

– The three cD galaxies (GMP 3329/NGC 4874, GMP 2921/NGC 4889, GMP 4928/NGC 4839);
– The first four most luminous E and S0s;
– One E and one S0 every three going down the luminosity function to $R_{KC_T} = 14$ mag;
– All E/S0 intermediate types down to $R_{KC_T} = 14.06$ mag.

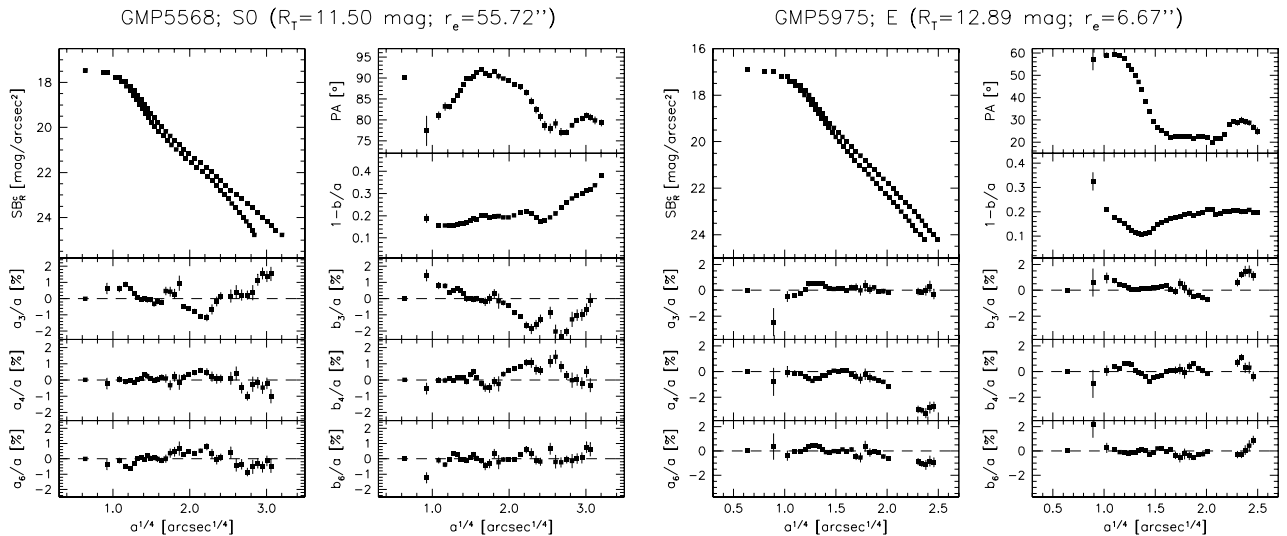For the outer region of the cluster ($D \geq 40'$) we selected all and 8 early type galaxies identified in Sect. 2 of this paper.

Table 1 lists all galaxies of the selected spectroscopic sample and their photometric properties. Numeros 1–27 correspond to the inner sample: The photometric total gunn r magnitude from JK94 is converted to Kron-Cousins R_{KC_T} using $R_{KC} = r - 0.35$ (see Jørgensen 1994; J94). Additionally the seeing corrected values for the effective radius r_e and the mean surface brightness $\langle SB_e \rangle$ inside r_e from Jørgensen et al. (1995a, JFK95a) are listed. Different to BM87's approach, JK94 derived the fourth cosine coefficients c_4 normalized to the equivalent radius $r = \sqrt{ab}$ where a and b are the semi-major and -minor axes. Hence the relation between a_4, which is normalized to the semi-major axis, and c_4 is

$$a_4 = c_4 \times \sqrt{1 - \epsilon}, \tag{2}$$

where a_4, c_4, and ϵ are the Fourier coefficients and the ellipticity at the current semi-major axis, respectively. Since JK94 only give the intensity weighted $\langle c_4 \rangle$ values and the ellipticity ϵ_{r_e} at r_e we could not derive the intensity weighted $\langle a_4 \rangle$ values by combining Eqs. (1, 2). Instead

we converted the available $\langle c_4 \rangle$ values into $\langle a_4 \rangle$ using the relation

$$\langle a_4 \rangle = \langle c_4 \rangle \times \sqrt{1 - \epsilon_{r_e}}, \tag{3}$$

which are listed in Table 1. For galaxies with $\epsilon = 0.1$ to 0.8 and $a_4 = -0.8$ to $+0.9$ we tested how well this conversion works. It turned out that the difference of $\langle a_4 \rangle$ derived by Eq. (3) on the one side and by combining Eqs. (1, 2) on the other side is smaller than 0.02% on the mean, which is much smaller than the typical error of $\langle a_4 \rangle$. ϵ_{r_e} from JK94 and the galaxy type given from D80 are also given in Table 1. Numeros 28–35 of Table 1 correspond to the outer sample and contain the parameter derived in Sect. 2 for the 8 identified early-type galaxies.

Comparison with the catalogue of JF94 shows that our inner sample (Nos. 1–27 in Table 1) is complete to $R_{KC_T} = 12.63$ mag and 42% complete in the range 12.63 mag $< R_{KC_T} < 14.06$ mag corresponding to a limiting absolute magnitude of $M_R > -21.73$ mag ($H_0 = 50$ Mpc/km s^{-1} and $cz_{CMB} = 7200$ km s^{-1}). The outer sample (Nos. 28–35 in Table 1) is complete to $R_{KC_T} = 13.21$ mag. The mean effective radius of the sample is $\langle R_e \rangle = 13.1''$, the average effective surface brightness $\langle SB_e \rangle = 19.9$ mag/arcsec^2, the mean ellipticity $\langle \epsilon \rangle = 0.32$; 40% of the galaxies have significant *disky* ($a_4/a \geq +0.5$) isophotes on the mean, while only two objects (6%) have significant *boxy* ($a_4/a \leq -0.5$) isophotes. The isophotes of the remaining 54% do not deviate significantly from pure ellipses. The sample spans 3.1 decades in cluster density. Figure 2 shows the histogram of galaxy types as a function of the projected cluster distance D. Figure 3 shows the magnitudes of the galaxies as a function of D.

4. Spectroscopic observations and data reduction

Long-slit spectra centered on the 5170 Å Mg triplet of the galaxies were taken along their major axes. Table 2

Table 1. The galaxies of the sample: GMP No., the number from GMP83; DN, numbers from Dressler (1980, D80); D, distance from the cluster center ($\alpha = 12{:}57.3$; $\delta = +28{:}14.4'$ (1950)) given by GMP83. Photometric parameter for object $1-27$ (inner sample): $R_{\mathrm{KC_T}}$, Kron-Cousin R band magnitude transformed from the Gunn r magnitudes quoted from JF94 using $R_{\mathrm{KC_T}} = r_T - 0.35\,\mathrm{mag}$ (see J94); r_e and $\langle SB_e \rangle$, seeing corrected effective radius and mean surface brightness within r_e from JFK95a; $\langle a_4 \rangle$, luminosity weighted mean a_4 parameter (defined by BM87) converted from the luminosity weighted mean $\langle c_4 \rangle$ from JK94 as described in the text; ϵ_{r_e}, ellipticity derived at r_e from JF94; type, galaxy classification from D80. Photometric parameter for objects $28 - 35$ (outer sample): $R_{\mathrm{c_T}}$, Kron-Cousin R band magnitude; r_e, $\langle SB_e \rangle$, a_4, ϵ_{r_e} and type derived from the data described in Sect. 2. ($*$) photometric zero point determined with HST V band surface photometry (Proposal ID: 5997). ($\triangle$) photometric zero point determined with surface photometry from GMP83

No.	GMP No.	NGC/IC No.	DN	D ['']	$R_{\mathrm{KC_T}}$ [mag]	r_e ['']	$\langle SB_e \rangle$ [mag/arcsec^2]	$\langle a_4 \rangle$ [%]	ϵ_{r_e}	Type
1	3329	NGC 4874	129	130.6	10.61	70.79	22.13	+0.1	0.141	D
2	2921	NGC 4889	148	304.8	10.64	33.88	20.64	-0.4	0.360	D
3	4928	NGC 4839	31	2528.4	11.45	29.51	21.18	±0	0.426	E/S0 (D)
4	4822	NGC 4841A	240	2533.4	11.78	17.87	20.39	−0.4	0.157	E
5	1750	NGC 4926	49	2111.2	12.27	10.96	19.79	−0.1	0.132	E
6	2390	IC 4051	143	927.7	12.34	15.56	21.02	±0	0.264	E
7	2795	NGC 4895	206	939.7	12.49	10.00	19.86	+0.9	0.599	S0
8	3792	NGC 4860	194	775.7	12.63	8.51	19.64	+0.2	0.161	E
9	2629	NGC 4896	232	1480.4	12.76	11.75	20.49	+0.7	0.424	S0
10	3561	NGC 4865	179	528.7	12.82	5.13	18.77	+0.6	0.429	S0
11	2000	NGC 4923	78	1480.8	12.86	8.51	19.88	+0.2	0.182	E
12	2413	-	230	1675.2	12.88	7.76	19.72	+0.5	0.405	S0
13	4829	NGC 4840	46	2184.3	12.93	6.46	19.35	+0.5	0.163	E/S0
14	3510	NGC 4869	105	359.6	12.93	7.59	19.75	+0.2	0.112	E
15	2417	NGC 4908	167	916.7	12.97	7.08	19.60	−0.2	0.322	S0/E
16	2440	IC 4045	168	945.9	13.24	4.37	18.79	+0.9	0.330	E
17	3414	NGC 4871	131	208.6	13.27	8.32	20.24	+1.1	0.410	S0
18	4315	NGC 4850	137	1104.0	13.36	4.68	19.07	+0.2	0.212	E/S0
19	3073	NGC 4883	175	271.4	13.36	6.91	19.91	+0.4	0.224	S0
20	1853	-	190	1674.6	13.45	4.27	18.96	+4.9	0.558	S0
21	3201	NGC 4876	124	210.2	13.51	5.13	19.47	±0	0.297	E
22	3661	-	13	2087.8	13.67	5.25	19.57	+0.3	0.264	S0
23	4679	-	75	1756.8	13.71	12.02	21.52	+2.6	0.789	S0
24	3352	NGC 4872	130	170.3	13.75	3.02	18.53	+0.6	0.054	E/S0
25	2535	IC 4041	145	742.0	13.81	7.41	20.52	+0.4	0.443	S0
26	3958	IC 3947	72	971.3	14.00	3.31	19.00	+1.6	0.323	E
27	2776	-	39	1567.4	14.06	5.76	20.25	+0.3	0.177	S0/E
28	0144	NGC 4957	–	4574.0	12.16*	18.44	20.38	+0.4	0.256	E
29	0282	NGC 4952	–	5849.3	12.03*	14.11	19.67	+0.9	0.315	E
30	0756	NGC 4944	–	33294	12.48△	11.68	19.71	+0.7	0.657	S0
31	1176	NGC 4931	–	2601.1	13.21△	7.40	19.45	+3.1	0.552	S0
32	1990	-	–	4413.1	12.78△	9.45	19.55	−0.6	0.485	E/S0
33	5279	NGC 4827	–	3737.1	12.33*	13.61	19.90	+0.1	0.205	E
34	5568	NGC 4816	–	2937.6	11.50*	55.72	22.13	−0.1	0.284	S0
35	5975	NGC 4807	–	3764.5	12.89*	6.67	18.91	−0.8	0.170	E

describes the setups used during the 6 runs of observations at the 2.4 m telescope of the Michigan-Dartmouth-M.I.T. (MDM) observatory at Kitt Peak, the 2.7 m telescope at Mc Donald observatory (McD) and the 3.5 m telescope of the German-Spanish Astronomical Center on Calar Alto (CA). Table 3 gives the log of the observations. Depending on the telescope the seeing was either measured by a seeing monitor or by measuring the point spread function (PSF) of a star image in the beginning of the night and controlling it via the guiding probe. The seeing listed in Table 3 is the worst value measured for the individual exposures. As we also needed "velocity standard" stars to determine the kinematical parameters of the galaxies, we obtained spectra for several G9 to K1 – giant template stars for all three setups. To make sure that the illumination across the slit was uniform and like in the galaxies we trailed and wiggled the stars across the slit. This ensured that the instrumental broadening was always the same in the stars as in the galaxies. For the kinematic analysis itself we finally only used spectra of HR 6817 (K1III) and HD 172401
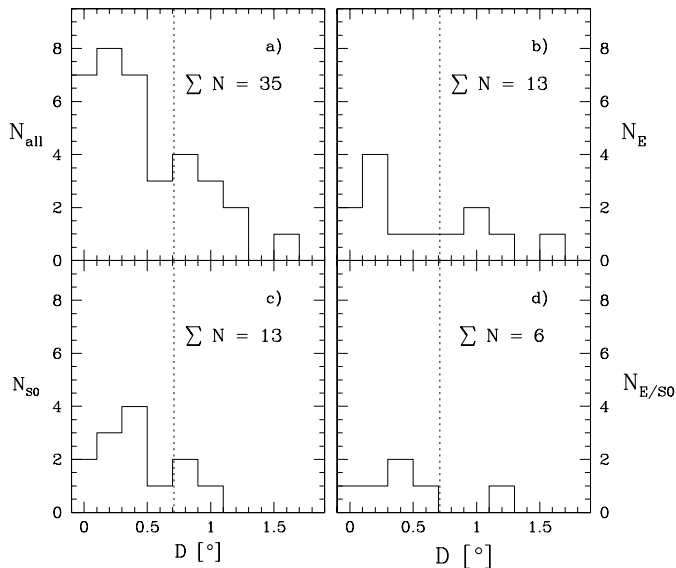
Fig. 2. The distribution of galaxies as a function of the projected distance D from the cluster center. **a)** all galaxies; **b)** Es; **c)** S0s; **d)** E/S0. Galaxies with $D > 0.71°$ (dashed line) belong to the outer Sample

Fig. 3. The total galaxy magnitude R_{KC_T} as a function of the projected distance D from the galaxy center. Filled triangles indicate cDs, open squares Es, open triangles S0s, open stars E/S0s. Galaxies with $D > 0.71°$ (vertical dotted line) belong to the outer sample. The long-dashed line indicates the completeness limit of the inner sample ($R_{KC_T} = 12.63$; horizontal dashed line)

(KOIII) both from Gonzales (1993, G93). Additionally we observed the flux standard star G191B2B or HD 19228 to calibrate the flux of the spectra before line strength indices were derived. The standard reduction (bias & dark subtraction, flat fielding, wavelength calibration, cleaning for cosmics, sky subtraction, correction for CCD misalignment) was carried out with our own programs running under the image processing package MIDAS provided by ESO and which are described in details in Bender et al. (1994, BSG94). Finally multiple exposures for one galaxy were centered and summed up to increase the final signal-to-noise.

The pixel-to-pixel noise in the normalized flat field is $< 0.2\%$. A sky subtraction better than 1% was achieved, while the errors in the wavelength calibration were $\leq$ 0.15 Å. The variation of the spectral resolution with λ was also ≤ 0.15 Å and stable during each observing run ($\delta\lambda \leq 0.05$ Å).

The quality of the final spectrum – and hence the resulting S/N – depends on the spectral resolution, the efficiency of the spectrograph as well as on the seeing conditions. Figure 4 shows examples of central spectra covering the 3 quality classes listed in Table 3 for the different instrumental resolutions σ_{inst}. The spectra are averaged within the radius r_L, which corresponds to a circular standard aperture having a diameter of $2r_A = 3.4''$ (see Sect. 5). For $\sigma_{inst} = 67.9$ km s^{-1} (run 2, 3, 5, 6), the quality parameter is either 1 or 2, while for $\sigma_{inst} = 129.4$ km s^{-1} (run 1 & 4) it is only 2 or 3. Because of the low instrumental resolution we excluded the latter ones from having quality 1 by default.
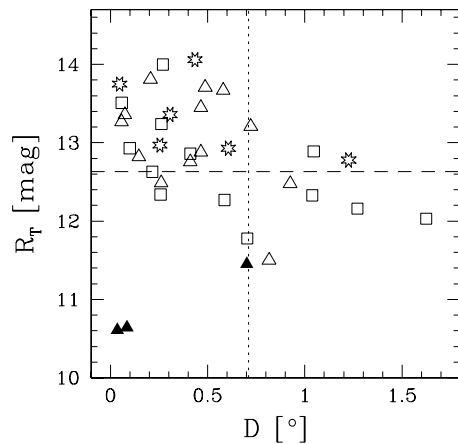
In the next step the spectra were rebinned along the slit (spatial direction) to achieve a minimum signal-to-noise (S/N) ≥ 40/Å at all radii (for details of the procedure see BSG94). Of course the central pixels have higher S/N (up to a factor of 5). Monte Carlo simulations described by BSG94 showed that a minimum on $S/N = 30 - 40$ is necessary to derive meaningful kinematical parameters with negligible systematic errors. As a final step of the pre-processing, the galaxy continuum was removed by fitting a forth to sixth order polynomial. We then determined the line-of-sight-velocity-distributions (LOSVDs) by using the Fourier Correlation Quotient (FCQ) method (Bender 1990), which provides the stellar rotational velocities v_{rot}, velocity dispersions σ and first orders of asymmetric (H_3) and symmetric (H_4) deviations of the LOSVDs from real Gaussian profiles (van der Marel & Franx 1993; Gerhard 1993; BSG94). As expected, we find that the FCQ method is little influenced by template mismatching (Bender 1990). Following BSG94, Monte Carlo simulations were made to find the best fit-order for the continuum and to check for systematic effects. It turns out that for runs 2, 3, 5, and 6, which have high spectral resolution there are no systematic errors for all kinematic parameters. Even for runs 1 & 4, that have rather low spectral resolution (129.4 km s^{-1}), v_{rot}, σ and H_3 do not show any systematic errors. Only the derived H_4 amplitude for this setup turns out to be systematically negative for $S/N \leq 80$. At $S/N = 40$ the systematic error is -0.04 and hence is of the order of the error bars (see below). We corrected for this systematic error using the dependence of H_4 on S/N delivered by the Monte Carlo simulations. The error bars were derived from photon statistics and CCD read-out noise and were calibrated via Monte Carlo
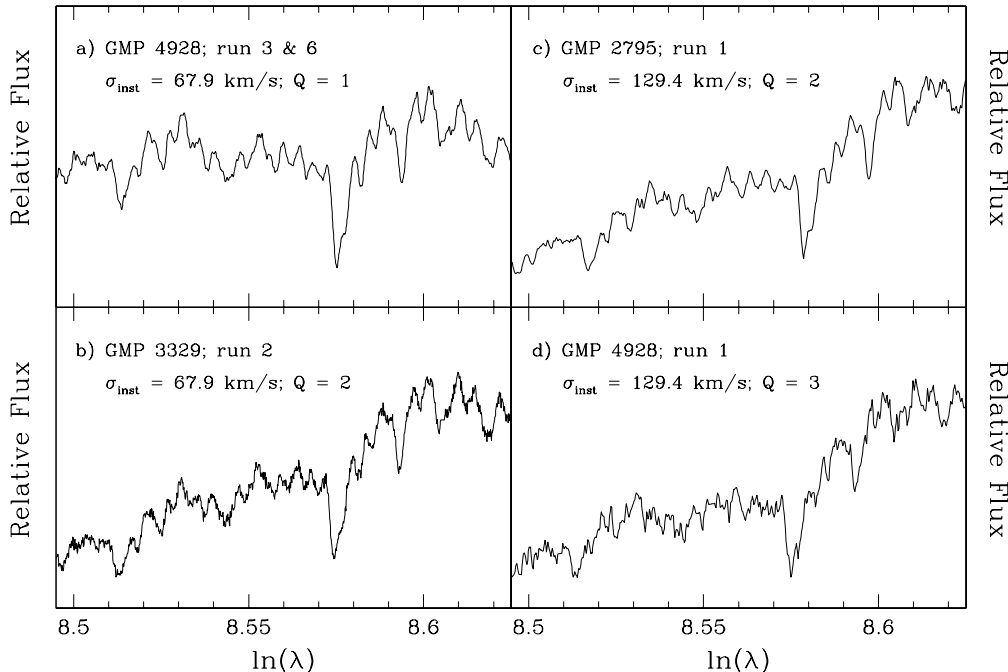
Fig. 4. Example spectra averaged within a circular standard aperture (see text) covering the range of quality classes for different instrumental resolutions: **a)** and **b)** show spectra with high instrumental resolution ($\sigma = 67.9$ km s^{-1}) having very good (1) and good (2) quality. There are no spectra of quality worse than two for this instrumental resolutions. **c)** and **d)** show spectra with low instrumental resolution ($\sigma = 129.4$ km s^{-1}) having good (2) and fair (3) quality. Because of the low instrumental resolution we excluded the latter ones to have quality 1 by default. Note that the panels show relative flux and have a false zero point for viewing convenience

simulations described by Gerhard et al. (1998): Noise is added to template stars, broadened following the observed values of H_4 and σ, matching the power spectrum noise to peak ratio of the galaxy. The accuracy of the estimated error bars is about 20%.

Additionally we tested whether our estimated kinematic errors indeed reproduce the RMS scatter between different exposures of the same galaxy. For all setups the expected errors – derived via our Monte Carlo simulations and shown in Fig. 6 – are of the order of the RMS. In fact for most galaxies the errors were slightly larger than the RMS by a factor of ≈ 1.2. In a few cases the estimated errors were overestimated up to a factor of 2.

Mg, Fe and Hβ line strength indices were derived following Faber et al. (1985) and Worthey (1992) from flux calibrated spectra, rebinned radially as before. For the 11 galaxies observed with the MDM setup (run 1 and 4), that covers a larger λ range, we could in addition derive the NaD line index profiles. We corrected all measured indices for velocity dispersion broadening and calibrated our measurements to the Lick system using stars from Faber et al. (1985). The errors are derived from photon statistics and CCD read-out noise. As for the kinematic parameters we tested whether our estimated errors indeed reproduce the RMS scatter between different exposures of the same galaxy. Again, for all setups the estimated errors – derived via our Monte Carlo simulations and shown in Fig. 6 – are

of the order of the RMS. For most galaxies the errors were slightly larger than the RMS by a factor of ≈ 1.2 and in a few cases the estimated errors were overestimated up to a factor of 2.

In the following we indicate the average Iron index with $\langle \text{Fe} \rangle = (\text{Fe}_{5270} + \text{Fe}_{5335})/2$ (Gorgas et al. 1990) and the usual combined Magnesium-Iron index with $[\text{MgFe}] = \sqrt{\text{Mg}b\langle\text{Fe}\rangle}$ (G93).

Some of the line index profiles needed further treatment. At small radii some of them show unreal features caused by the varying focus of the spectrograph in the dispersion direction. Following G93, this effect is only detectable if the variation of the focus' point spread function (PSF) is dominant compared to the atmospherical seeing (FWHM). For some of the galaxies the focus variation was the dominant effect and we followed the procedure described in Mehlert et al. (1998, MSBW98) to correct it. The Mg$_1$ and Mg$_2$ indices defined by Faber et al. (1985) are affected most, because their pseudo continua are ≈ 200 Å apart from the line windows. For all the other line indices the continuum and line windows are close to each other. Hβ and the Fe indices are in the red and blue part of the spectra and thus slightly affected, while the Mgb index at the central wavelength is almost unaffected.

Recent investigations showed evidence for small amount of ionized gas and dust in the interstellar medium

(ISM) of many elliptical galaxies (e.g. Bregman et al. 1992; Goudfrooij et al. 1994). Consequently, the detection of some emission (e.g. Hβ, N, and O) in their spectra is expected. Since the velocities of the stars and gas in the galaxies may differ by up to 100 km s^{-1} (Bertola et al. 1995) asymmetric contamination of line indices is possible. In addition the dust and ionized gas show a wide range of distribution: Smoothly along their major/minor axis or in rather patchy or filamentary features (Goudfrooij et al. 1994). If one wants to investigate the stellar population of elliptical galaxies (as we are going to do in Paper II) the contamination of Hβ by emission is especially crucial. Emission will weaken the age indicating Hβ absorption index and hence lead to an overestimate of the age of the dominant stellar population (see Worthey 1994, W94). Simulations with the kinematical template stars we used showed that we can detect emission in Hβ for equivalent width larger than about 0.3 Å. Figure 5 shows examples of the strong (a) and weak (b) Hβ emission seen in the our spectra. We will refer to these two classes in the comments on the galaxies given in Sect. 5. In particular Fig. 5a demonstrates how asymmetric Hβ emission can be. Since no OIII emission is detected in this galaxy (GMP 4315) at all, these data illustrate that it is impossible to correct for Hβ emission via OIII as suggested by G93.

Additionally Goudfrooij & Emsellem (1996) showed that NI emission may influence the measured Mg indices (Δ Mgb up to 0.5 Å and Δ Mg$_2$ up to 0.03 mag). The influence of asymmetric NI emission can be seen in the Mgb profile of GMP 2390 (galaxy 6 in Fig. 6).

5. The spectroscopic database

The plots of Fig. 6 show the kinematic and line index profiles of the 35 Coma galaxies. The line of sight mean velocity $v(r)$, line of sight velocity dispersion $\sigma(r)$, third ($H_3(r)$) and fourth ($H_4(r)$) order coefficient of the Gauss-Hermite decomposition of the line of sight velocity distributions are given, as well as the profiles of the line indices Mgb, $\langle$Fe$\rangle$, [MgFe] and Hβ as a function of the radial distance r. All profiles are folded with respect to the galaxy center (v and H_3 are folded antisymetrically). The radial profiles of the Mg$_2$ index are only shown for data from run 3 and 6 (CA). No reasonable Mg$_2$ profiles could be derived from the McDonald (run 2 and 5) and MDM (run 1 and 4) data since these spectra were strongly distorted by the varying focus of the spectrograph and no satisfactory correction could be applied. For the 11 galaxies observed at MDM the additionally derived NaD line index profiles are also show in Fig. 6. The shown Hβ indices are not corrected for emission as suggested by G93 (see Sect. 4). The numerical values of these radial profiles are also listed in Tables 13 to 82 in Appendix B.

Different radial binnings for kinematic parameters and line indices occur for two reasons: On the one hand we
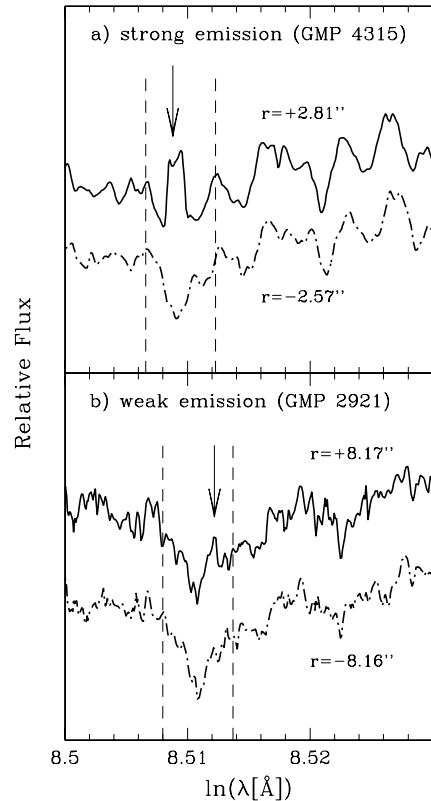

Fig. 5. Examples of the two classes of Hβ emission strength detected in our spectra (solid line): **a)** strong and **b)** weak emission. For comparison we also show the Hβ absorption line at the opposite sides of the galaxies, where no emission is detected (dashed-dotted line). The vertical dashed lines indicate the redshifted position of the Hβ absorption window. The arrow indicates the position of the detected emission. In particular panel **a)** also shows the strong asymmetry of the Hβ absorption in GMP 4315. While strong Hβ emission exists at $r = +2.81''$, there is none at all at the opposite side of the galaxy ($r = -2.57''$; dashed-dotted line). Since no OIII emission is detected in this galaxy at all, these data also demonstrate, that it is not possible to correct for Hβ emission via OIII. Note that the panels show relative flux and have a false zero point for viewing convenience

used different wavelength range for the kinematic and the absorption index analysis. Hence a variation in the radial dependent S/N and consequently a different radial binning could occur. Additionally, for some galaxies the radial profile was focus corrected before deriving line indices. This also influences the radial S/N and hence the radial binning for the line index profiles.

For all 27 galaxies of the inner sample Jørgensen (1999, J99) lists aperture corrected, central σ and Mg$_2$[2] values from her own observations and the literature inside a standard aperture of diameter of $2r_A = 3.4''$. For 26 of this galaxies she also gives equivalent central Hβ indices as

---

[2] As already mentioned we could only derive reasonable Mg$_2$ profiles for 8 galaxies.

Table 2. Setups of the spectroscopic runs. The spectral resolutions in km s^{-1} were derived at the 5170 Å Mg triplet

Run	Date	Telescope	Detector Spectrograph	λ – range [Å]	Scale ["/pix]	Slit-width	spectral resolution [σ]
1 4	3/95 3/96	MDM 2.4 m	TI: 1024 × 1024 Mark III	4300–6540	0.777	1.7″	2.23 Å 129.4 km s^{-1}
2 5	4/95 4/96	McD 2.7 m	TI: 800 × 800 LCS	4850–5560	0.635	2.5″	1.17 Å 67.9 km s^{-1}
3 6	5/95 5/96	CA 3.5 m	TI: 1024 × 1024 TWIN/R	4730–5700	0.896	3.6″	1.17 Å 67.9 km s^{-1}

well as equivalent central Mgb and <Fe> indices for 20 of them. Following Jørgensen et al. (1995b, JFK95b), we converted the aperture radius r_A in the "slit-equivalent" radius r_L using the formula $r_L = (\frac{r_A}{1.025})^2 \frac{\pi}{2b}$, where b is the slit width. With the given slit width in Table 3 r_L is 1.2″, 1.7″ and 2.5″ for the CA, McD and MDM setup, respectively. Overplotted in Fig. 6 we show these aperture corrected mean values from J99 at the "slit-equivalent" radii r_L. No central values are available for the 8 galaxies of the outer sample. In Sect. 6 we will discuss the comparison of our data with those available in literature in details.

Comments on the radial profiles of some galaxies are given in the following. Examples of the used classes of the Hβ emission strength are given in Fig. 5.

Comments on single galaxies:

(1) cD Galaxy GMP 3329 (NGC 4874): Weak, asymmetric NI emission contaminates the Mgb index at $r \approx 5″ - 8″$. Weak Hβ emission contaminates the Hβ absorption index at $r \approx 8″ - 12″$. The mean Hβ index from J99 is significantly lower compared to our profile.

(2) D Galaxy GMP 2921 (NGC 4889) Weak Hβ emission contaminates the Hβ absorption index in the center and at $r \approx 8″$. The Mgb peak at $r \approx 4″$ is real as well as the differences of the $\langle$Fe$\rangle$ index at different sides of the galaxy. There is no evidence for further emission or systematic errors in the continuum shape.

(3) cD Galaxy GMP 4928 (NGC 4839) (SW): A foreground object existing between $+16″$ and $+22″$ has been excluded from the analysis. Weak Hβ emission contaminates the Hβ absorption index at radii > 25″.

(4) GMP 4822: Weak Hβ emission contaminates the Hβ absorption index at radii > 6″.

(6) GMP 2390: This galaxy hosts a kinematically decoupled, co-rotating core (see MSBW98). Weak, asymmetric NI emission contaminates the Mgb index inside 3″. Slight Hβ emission contaminates the Hβ absorption index at radii > 10″.

(7) GMP 2795: Weak Hβ emission contaminates the Hβ absorption index at 2″ − 4″. The mean σ from J99 is sig-

nificantly lower compared to our profile.

(8) GMP 3792: The inner "bump" of the $\langle$Fe$\rangle$ index is caused by the varying focus of the spectrograph and could not be corrected sufficiently.

(9) GMP 2629: The mean Hβ index from J99 is significantly higher compared to our profile, while σ is significantly lower.

(11) GMP 2000: Weak Hβ emission contaminates the Hβ absorption index at $3″ - 6″$.

(12) GMP 2413: Weak, asymmetric NI emission contaminates the Mgb index at 1″. The inner "bump" of the $\langle$Fe$\rangle$ index is caused by the varying focus of the spectrograph and could not be corrected sufficiently.

(15) GMP 2417: The mean Hβ index from J99 is significantly higher compared to our profile.

(18) GMP 4315: This galaxy shows strong and asymmetric Hβ emission, which is demonstrated in Fig. 5a. Since no OIII emission is detected at all, these data clearly demonstrate that it is not possible to correct for Hβ emission via OIII by applying the method suggested by G93.

(19) GMP 3073: The mean Hβ and $\langle$Fe$\rangle$ indices from J99 are significantly higher compared to our profiles.

(20) GMP 1853: The mean σ and $\langle$Fe$\rangle$ indices from J99 are significantly higher compared to our profiles.

(21) GMP 3201: Weak Hβ emission contaminates the Hβ absorption index at radii > 3.5″.

(22) GMP 3661: The $\langle$Fe$\rangle$ index profiles could not be corrected perfectly for the focus variation of the spectrograph.

(23) GMP 4679: The asymmetry in the $\langle$Fe$\rangle$ index is real. There is no evidence for emission or systematic errors in the continuum shape.

(24) GMP 3352: The Mgb and $\langle$Fe$\rangle$ index profiles could not perfectly be corrected for the focus variation of the spectrograph. The mean Hβ index from J99 is significantly lower compared to our profile.

(25) GMP 2535: Weak Hβ emission contaminates the Hβ absorption index at radii > 4″.

(26) GMP 3958: The mean Hβ index from J99 is significantly higher compared to our profiles.

(27) GMP 2776: The mean $\langle$Fe$\rangle$ index from J99 is significantly higher compared to our profiles.

Table 3. Log of the spectroscopic observations. Galaxy numbers as in Table 1. For galaxy No. 3 the spectra from run 3 and 6 are summed up; for galaxy Nos. 9 and 12 the spectra from run 1 and 4 are summed up. The seeing has been measured for each single exposure. The maximum value detected in the most broadend spectrum for one galaxy is listed. The parameter Q estimates the quality of the spectra: 1, very good; 2, good; 3, medium (see Fig. 4)

No.	GMP No.	NGC/IC No.	DN	Run	Single exp. times [s]	Total exp. times [s]	PA (N $\geq$ E)	Seeing (FWHM)	Q
1	3329	NGC 4874	129	2	3×3600	10800	45°	1.8″	2
2	2921	NGC 4889	148	2	$2 \times 3600 + 1800$	9000	81°	2.2″	2
3	4928	NGC 4839	31	1	2×3600	7200	63°	1.8″	3
				2	$2 \times 2700 + 3350$	8750	63°	2.0″	3
				3	1800		63°		1
				6	1800	3600	63°	2.8″	1
4	4822	NGC 4841A	240	1	$2 \times 3600 + 2400$	9600	105°	1.5″	2
5	1750	NGC 4926	49	1	$3600 + 4500 + 2700$	10800	60°	1.8″	2
6	2390	IC 4051	143	1	$2 \times 3600 + 2000 + 1600$	10800	106°	1.8″	2
7	2795	NGC 4895	206	1	3×3600	10800	156°	1.5″	2
8	3792	NGC 4860	194	1	$3600 + 1520 + 3000 + 2400$	10520	127°	1.4″	2
9	2629	NGC 4896	232	1	$2 \times 3600 + 2010$		7°		2
				4	$3000 + 2850$	15060	7°	1.8″	2
10	3561	NGC 4865	179	1	$3 \times 3000 + 1800$	10800	115°	1.8″	2
11	2000	NGC 4923	78	3	2×3600	7200	77°	2.2″	1
12	2413	–	230	1	$2700 + 2050 + 3000$		25°		2
				4	2×3000	13750	25°	1.8″	2
13	4829	NGC 4840	46	1	3×3300	9900	106°	1.5″	2
14	3510	NGC 4869	105	3	2×3600	7200	169°	2.5″	1
15	2417	NGC 4908	167	3	2×3600	7200	55°	2.5″	1
16	2440	IC 4045	168	3	$2300 + 2500 + 2000$	6800	108°	2.2″	1
17	3414	NGC 4871	131	3	$3120 + 3200 + 2400$	8700	178°	2.8″	1
18	4315	NGC 4850	137	3	2×3600	7200	153°	2.2″	1
19	3073	NGC 4883	175	3	2×3600	7200	106°	2.2″	1
20	1853	–	190	4	3×3600	10800	88°	1.6″	2
21	3201	NGC 4876	124	4	$2 \times 4500 + 3600$	12600	24°	1.7″	2
22	3661	–	13	5	$4 \times 3600 + 2400$	16800	139°	1.4″	1
23	4679	–	75	5	$2 \times 4800 + 5700$	15300	114°	1.6″	1
24	3352	NGC 4872	130	5	$2 \times 5400 + 3600$	14400	111°	1.5″	1
25	2535	IC 4041	145	5	3×4800	14400	48°	1.3″	1
26	3958	IC 3947	72	5	3×4800	14400	102°	1.5″	1
27	2776	–	39	5	3×4800	14400	77°	2.3″	1
28	0144	NGC 4957	–	6	$4300 + 4500$	8800	91°	1.5″	1
29	0282	NGC 4952	–	6	$4100 + 5000$	9100	135°	2.5″	1
30	0756	NGC 4944	–	6	2×4500	9000	88°	2.0″	1
31	1176	NGC 4931	–	6	2×4500	9000	78°	2.0″	1
32	1990	–	–	6	$5100 + 4500$	9600	135°	2.2″	1
33	5279	NGC 4827	–	6	$4500 + 5330$	9830	56°	1.5″	1
34	5568	NGC 4816	–	6	$3600 + 3400$	7000	78°	1.2″	1
35	5975	NGC 4807	–	6	$4500 + 3000$	7500	23°	2.0″	1

(34) GMP 5568: This galaxy hosts a kinematically decoupled, counter-rotating core (see MSBW98).

6. Comparison with literature

Kinematical radial profiles for the three cD galaxies GMP 3329 (NGC 4874), GMP 2921 (NGC 4889) and GMP 4928 (NGC 4839) have already been measured by Davies & Illingworth (1983), Davies & Birkinshaw (1988) and Fisher et al. (1995). Figures 7, 8 and 9 show the comparison with our profiles. No systematic differences are found inside the error bars, except for the center of GMP 2921 (NGC 4889), where the difference in spectral resolution and slit width could be responsible for the discrepancies observed.
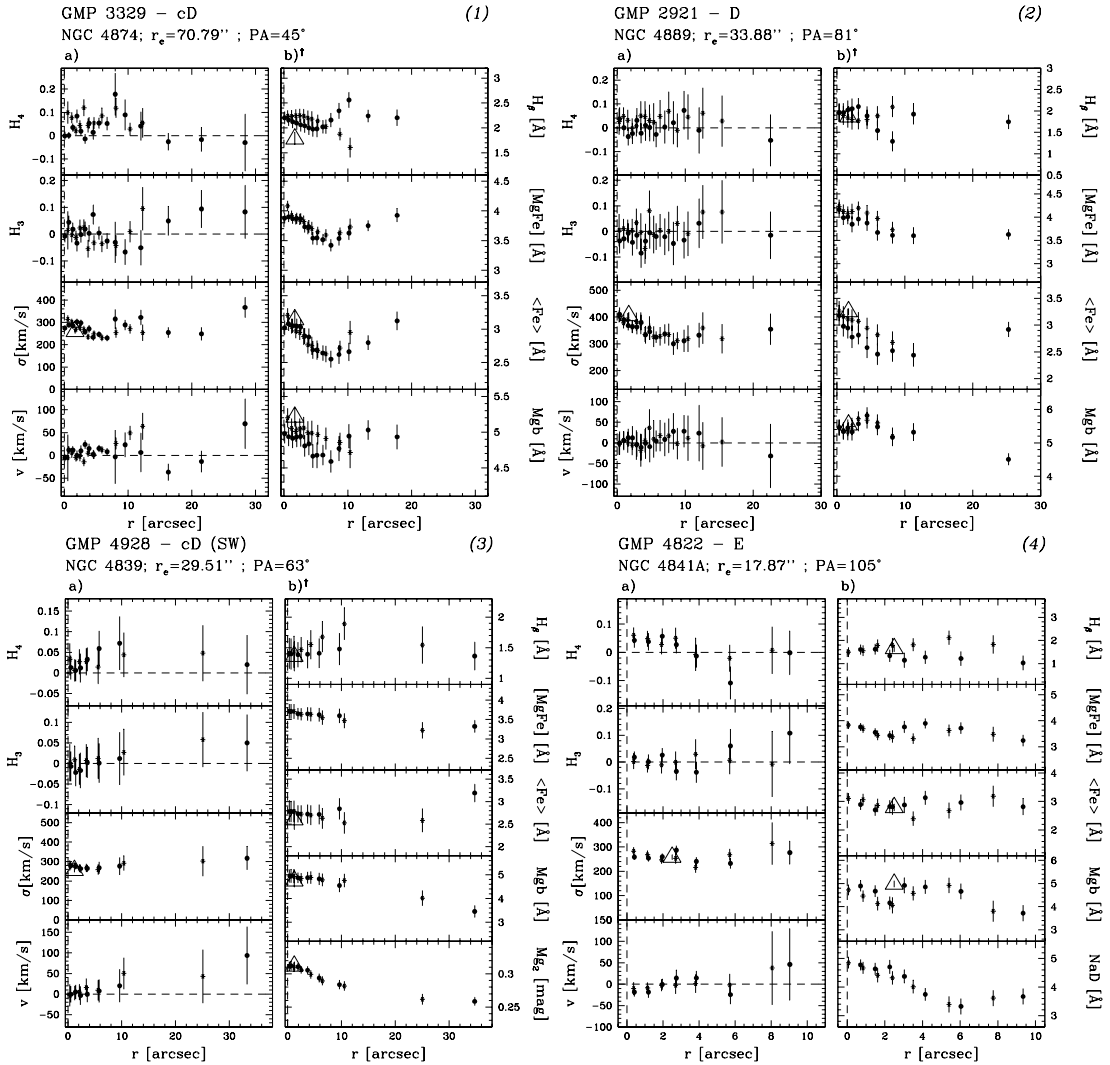
Fig. 6. a) Radial profiles of the kinematical parameters along the major axis (folded). From bottom to top: line of sight mean velocity $v(r)$, line of sight velocity dispersion $\sigma(r)$, third ($H_3(r)$) and fourth ($H_4(r)$) order coefficient of the Gauss-Hermite decomposition of the line of sight velocity distributions. **b)** Radial profiles of the line indices (from bottom to top) Hβ, [MgFe], $\langle$Fe$\rangle$ and Mgb. For a few galaxies either the Mg$_2$ or the NaD index profile is also shown. The symbol † indicates the index profiles where a focus correction has been applied. Because of this correction the profiles appear smoother and the error bars are sometimes larger than the internal scatter of the data. Filled circles and crosses refer to the two sides of the galaxy. Open triangles (when present) show aperture corrected values from J99 inside the standard circular aperture having a diameter of $3.4''$. Following JFK95b, we converted this aperture radius r_A in the "slit-equivalent" radius r_L (see text), which is $1.2''$, $1.7''$ and $2.5''$ for the CA, McD, and MDM setups, respectively. The vertical dashed line (when present) shows the position of $a_e = r_e/\sqrt{1 - \epsilon_{re}}$ indicating the half light radius projected to the observed major axis. The long-dashed horizontal line shows $r = 0$. Name, type, r_e and position angle of the galaxy are given at the top (left). The galaxy number indicated in Tables 1 and 3 are also shown at the top (right)

We also compared our velocity dispersion with the aperture corrected mean values from J99. Therefore we derived the mean values of our presented σ-profiles within the "slit-equivalent" radius (see Sect. 5). Figure 10 shows the difference between the mean values $\Delta(\log \sigma) = (\log \sigma)_{\text{thiswork}} - (\log \sigma)_{\text{J99}}$ versus our measured mean values inside the standard aperture. The RMS scatter as well as the mean difference are listed

in Table 4. No significant offset between the two datasets could be detected.

Radial line index profiles have been measured for the cD galaxies GMP 3329 (NGC 4874) and GMP 4928 (NGC 4839) by Fisher et al. (1995, FFI95) and Davies et al. (1993, DSP93). Figures 11 and 12 show the comparisons with our data. As FFI95 also derived
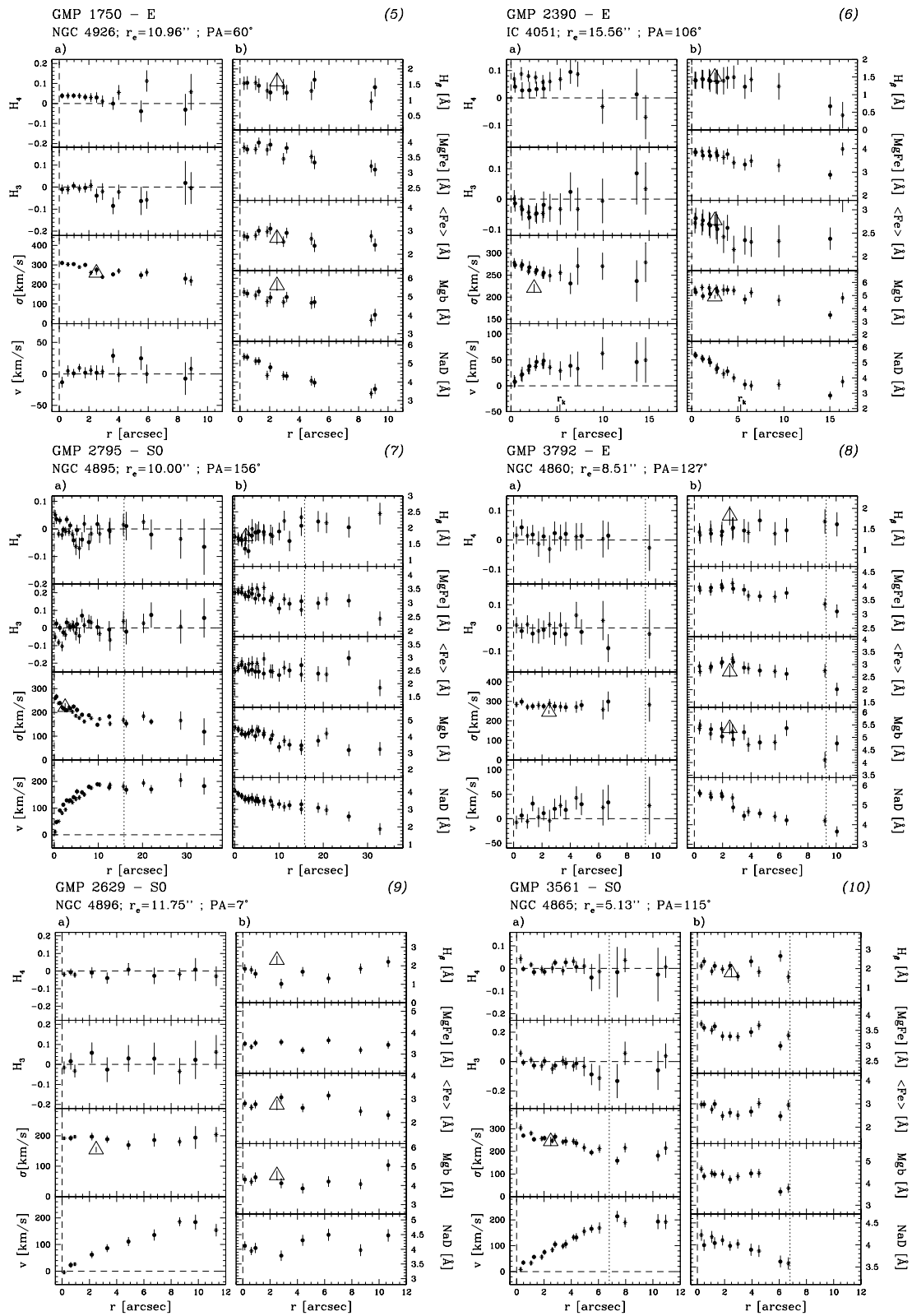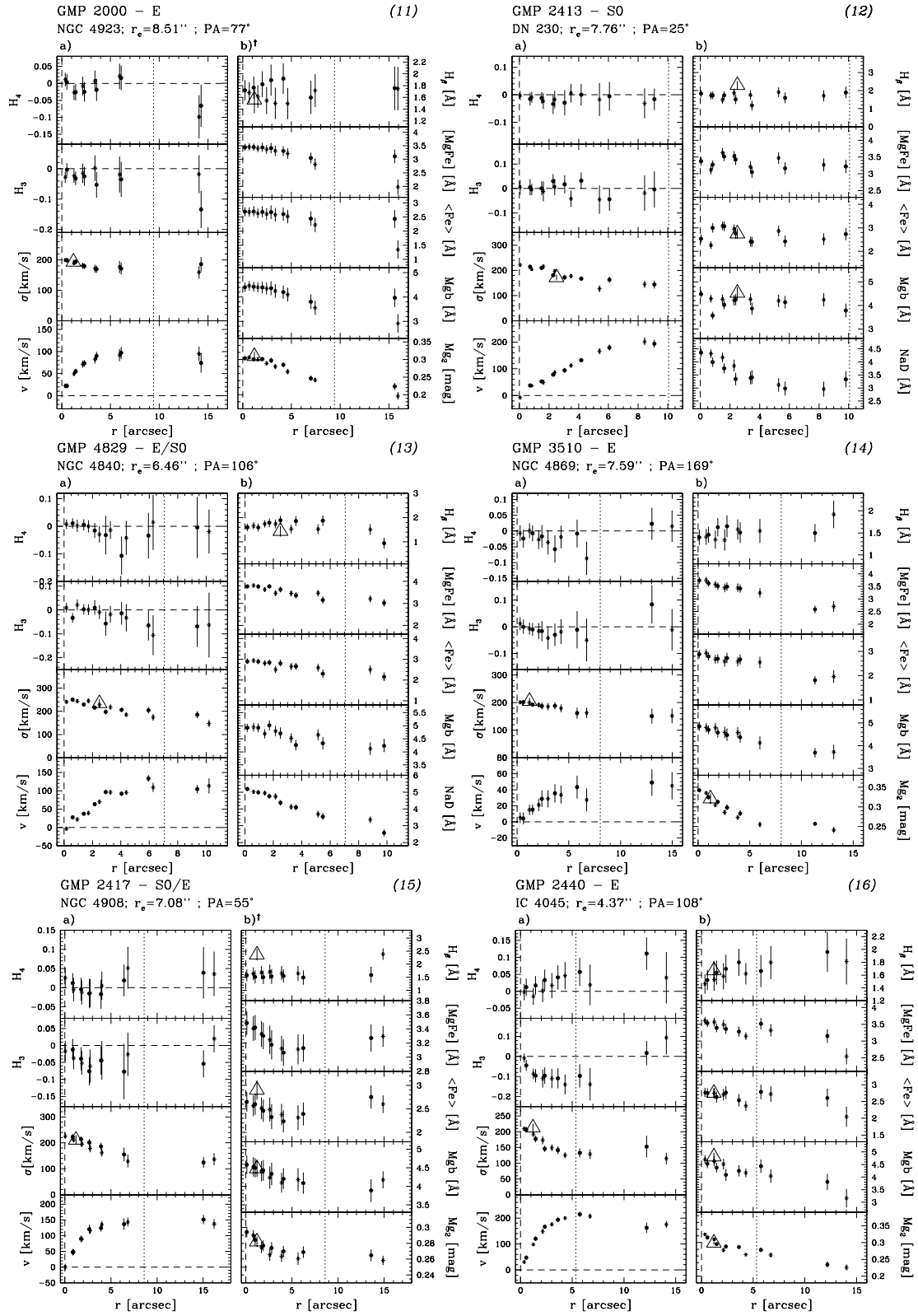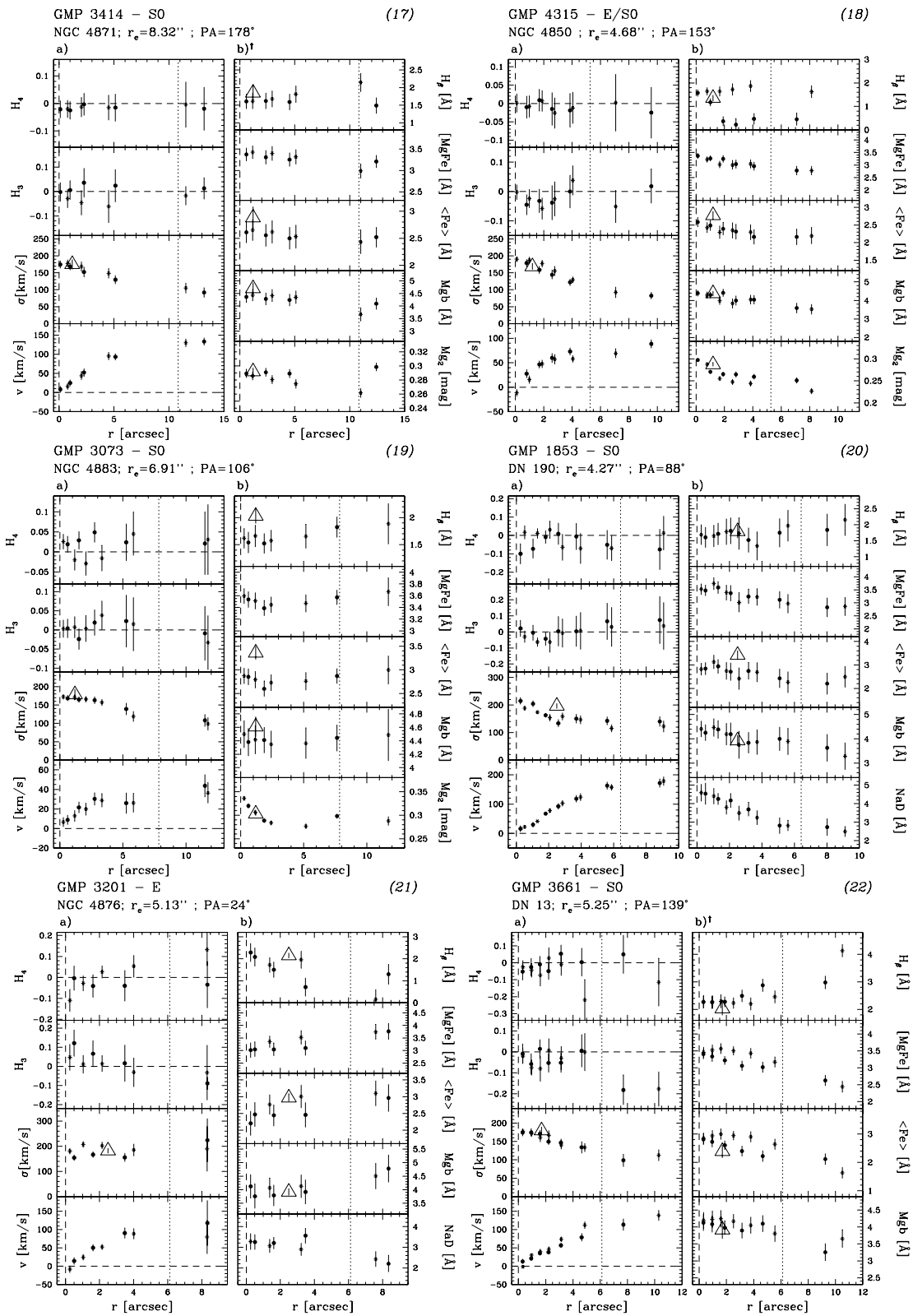
GMP 1750 – E   (5)
NGC 4926; r_e=10.96'' ; PA=60°

GMP 2390 – E   (6)
IC 4051; r_e=15.56'' ; PA=106°

GMP 2795 – S0   (7)
NGC 4895; r_e=10.00'' ; PA=156°

GMP 3792 – E   (8)
NGC 4860; r_e=8.51'' ; PA=127°

GMP 2629 – S0   (9)
NGC 4896; r_e=11.75'' ; PA=7°

GMP 3561 – S0   (10)
NGC 4865; r_e=5.13'' ; PA=115°

Fig. 6. continued

GMP 2000 – E   *(11)*
NGC 4923; r_e=8.51''; PA=77°

GMP 2413 – S0   *(12)*
DN 230; r_e=7.76''; PA=25°

GMP 4829 – E/S0   *(13)*
NGC 4840; r_e=6.46''; PA=106°

GMP 3510 – E   *(14)*
NGC 4869; r_e=7.59''; PA=169°

GMP 2417 – S0/E   *(15)*
NGC 4908; r_e=7.08''; PA=55°

GMP 2440 – E   *(16)*
IC 4045; r_e=4.37''; PA=108°

Fig. 6. continued

GMP 3414 — S0 *(17)*
NGC 4871; r_e=8.32'' ; PA=178°

GMP 4315 — E/S0 *(18)*
NGC 4850 ; r_e=4.68'' ; PA=153°

GMP 3073 — S0 *(19)*
NGC 4883; r_e=6.91'' ; PA=106°

GMP 1853 — S0 *(20)*
DN 190; r_e=4.27'' ; PA=88°

GMP 3201 — E *(21)*
NGC 4876; r_e=5.13'' ; PA=24°

GMP 3661 — S0 *(22)*
DN 13; r_e=5.25'' ; PA=139°

Fig. 6. continued

Fig. 6. continued

GMP 0282 – E   (29)
NGC 4952; r_e=14.11'' ; PA=135°

GMP 0756 – S0   (30)
NGC 4944; r_e=11.68'' ; PA=88°

GMP 1176 – S0   (31)
NGC 4931; r_e=7.40'' ; PA=78°

GMP 1990 – E/S0   (32)
--- ; r_e=9.45'' ; PA=78°

GMP 5279 – E   (33)
NGC 4827; r_e=13.61'' ; PA=56°

GMP 5568 – S0   (34)
NGC 4816; r_e=55.75'' ; PA=78°

Fig. 6. continued

Fig. 6. continued
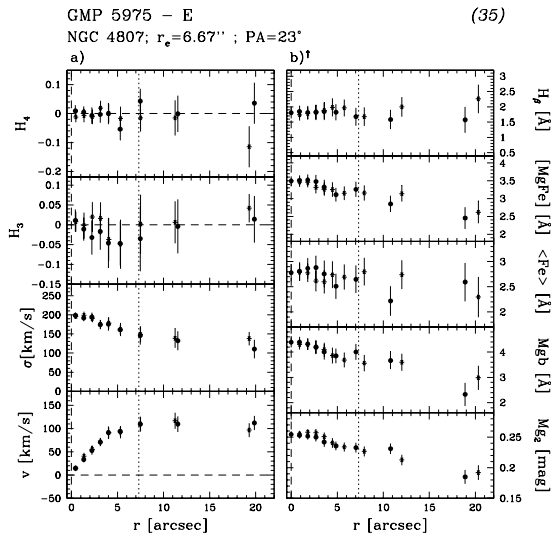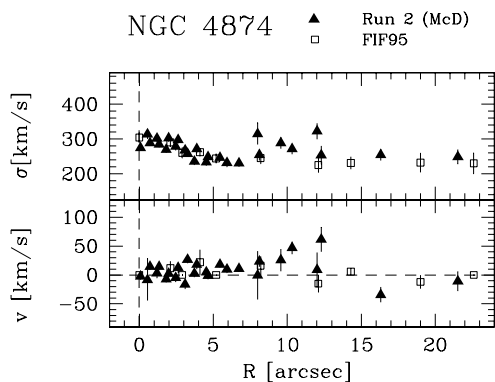
Fig. 7. The kinematical profile of GMP 3329 (NGC 4874) as measured during run 2 (spectral resolution $\sigma_{\rm inst} = 1.17$ Å, filled triangles) compared to the data of Fisher et al. (1995, spectral resolution $\sigma_{\rm inst} = 2.77$ Å, open squares). The data are folded with respect to the center and the same symbols are used for the two sides of the galaxies
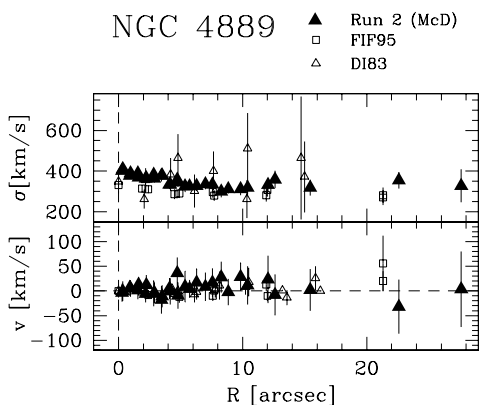
Fig. 8. The kinematical profiles of GMP 2921 (NGC 4889) as measured during run 2 (spectral resolution $\sigma_{\rm inst} = 1.17$ Å, filled triangles) compared to the data of Fisher et al. (1995, spectral resolution $\sigma_{\rm inst} = 4.68$ Å open squares) and the data of Davies & Illingworth (1983, spectral resolution $\sigma_{\rm inst} = 2.04$ Å, open triangles). The data are folded with respect to the center and the same symbols are used for the two sides of the galaxies
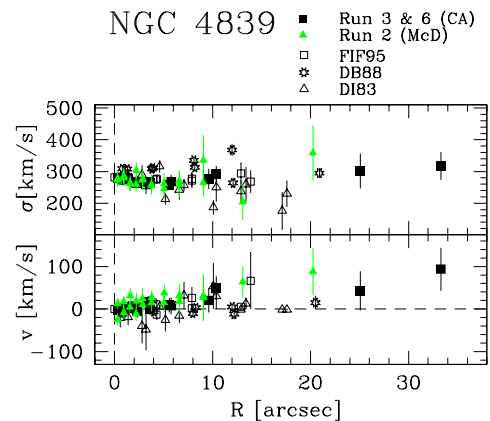

Fig. 9. The kinematical profiles of GMP 4928 (NGC 4839) as derived during runs 3 and 6 (spectral resolution $\sigma_{\rm inst} = 1.17$ Å, filled squares) and those from run 2 (spectral resolution $\sigma_{\rm inst} = 1.17$ Å, gray triangles) compared to the data of Fisher et al. (1995, spectral resolution $\sigma_{\rm inst} = 2.77$ Å, open squares), the ones of Davies & Birkinshaw (1988, spectral resolution $\sigma_{\rm inst} = 5.11$ Å, stars) and the ones of Davies & Illingworth (1983, spectral resolution $\sigma_{\rm inst} = 2.04$ Å, open triangles). The data are folded with respect to the center and the same symbols are used for the two sides of the galaxies

the Mg$_1$ index for GMP 4928 (NGC 4839) and the C4668[3] index, for both galaxies we also measured these indices for these two galaxies for comparison reasons. The Mg indices compare well with previous works. Strong systematic differences of unclear origin are seen when considering the Hβ profile of GMP 3329 (NGC 4874). The position angle of our observations at McD was the same as that used by FFI95. Hence the possibility of having investigated different areas of the galaxy can be ruled out as the reason. We also checked whether there is a systematic offset in our Hβ index measured from the McD data. This could also be excluded since the Hβ profile for the second comparison galaxy GMP 4928 (NGC 4839) derived from the McD data is not only consistent with our CA data for this galaxy, but also with results from FFI95 and DSP93 (Fig. 12). Hence we conclude that there should also be no systematic error in the Hβ index we derived for GMP 3329 (NGC 4874) from our McD data.

Additionally the C4668 profile of GMP 4928 (NGC 4839) derived by FFI95 shows a small systematic difference to our profiles derived from CA as well as McD data.

We also compared our measured indices with the aperture corrected mean values from J99. Again we derived the mean values of our presented index–profiles within the "slit-equivalent" radius (see Sect. 5). Figure 13 shows the difference between the mean values

---

[3] FFI95 as well as W94 called this index Fe4668. In publications after 1995 this index is C4668 as it turned out that it actually depends more on carbon than on iron.
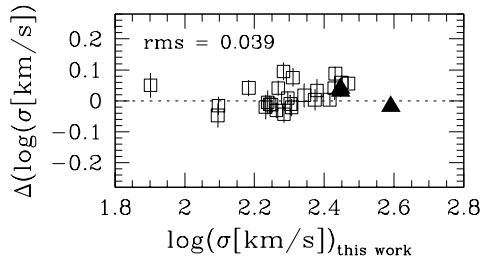
Fig. 10. Comparison between the velocity dispersion measured from our data and the aperture corrected mean values from J99, within the circular standard aperture having a diameter of $2r_A = 3.4''$. The "slit-equivalent" radius r_L is $1.2''$, $1.7''$ and $2.5''$ for the CA, McD, and MDM setup, respectively (see text). Filled triangles are the cD galaxies. Δ is calculated as "this work" - "literature"

Table 4. Results from the comparisons of our mean data within the circular standard aperture (see text) with the mean values given by J99. Δ is calculated as "this work" - "literature". Listed are the mean and the rms of Δ as well as its mean error. (∗) - J99 lists Mg_2 for all our 27 galaxies, but we could only derive reasonable radial profiles for the 8 galaxies observed during run 3 (see Sect. 4)

	N	$\langle\Delta\rangle$	rms (Δ)	$\langle err\rangle$
$\log\sigma$	27	0.017	0.039	0.028
Mgb	20	-0.08 Å	0.27 Å	0.25 Å
Mg_2	8∗	0.005 mag	0.010 mag	0.008 mag
$\langle Fe\rangle$	20	-0.11 Å	0.32 Å	0.22 Å
$H\beta$	26	-0.09 Å	0.35 Å	0.24 Å

Δ index = index$_{\text{thiswork}}$ − index$_{\text{J99}}$ versus our measured mean values inside the standard aperture. The rms scatter as well as the mean differences are listed in Table 4. No significant offset between the two datasets could be detected.

7. Conclusions

We have presented long-slit spectroscopy of 35 early-type galaxies of the Coma cluster. The high signal-to-noise of the data allowed us to derive *spatially resolved* spectra for a substantial sample of Coma galaxies for the first time. From these spectra we derived the kinematical profiles (line of sight velocities and velocity dispersions, third and fourth Hermite coefficients describing deviations from a purely Gaussian velocity distributions) and the radial line index profiles (Mgb, $\langle Fe\rangle$, $H\beta$) out to $1r_e - 3r_e$. CCD photometry for 8 early-type objects of the outer region of the cluster was also presented. The database will be used in future papers to study the stellar populations, their radial distribution and the dynamics of early-type galaxies as a function of cluster density.
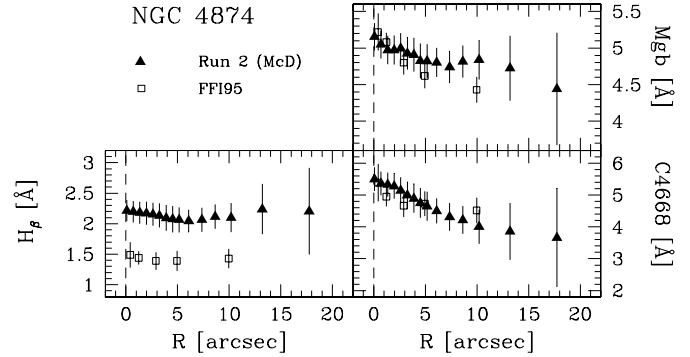
Fig. 11. The line index profiles of GMP 3329 (NGC 4874) as measured during run 2 (spectral resolution $\sigma_{\text{inst}} = 1.17$ Å, filled triangles) compared to the data of Fisher et al. (1995, spectral resolution $\sigma_{\text{inst}} = 2.77$ Å, open squared). The data are mean values for the two sides of the galaxies
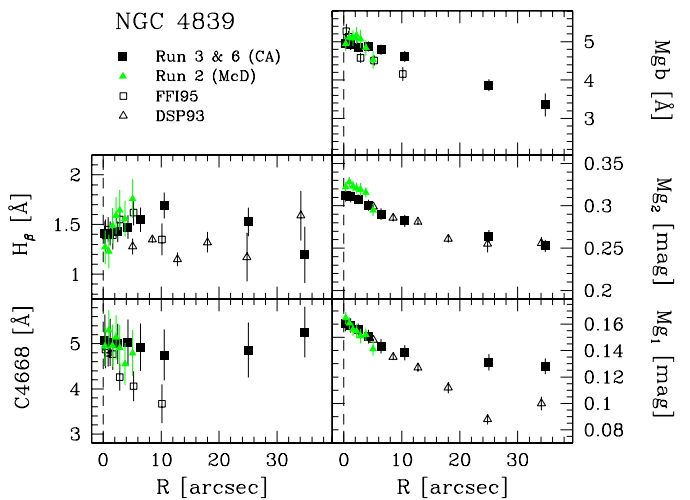

Fig. 12. The line index profiles of GMP 4928 (NGC 4839) as derived during runs 3 and 6 (spectral resolution $\sigma_{\text{inst}} = 1.17$ Å, filled squares) and those from run 2 (spectral resolution $\sigma_{\text{inst}} = 1.17$ Å, gray triangles) compared to the data of Fisher et al. (1995, spectral resolution $\sigma_{\text{inst}} = 2.77$ Å, open squares) and the ones of Davies et al. (1993, spectral resolution $\sigma_{\text{inst}} = 5.11$ Å, open triangles). The data are mean values for the two sides of the galaxies

References

Andreon S., Davoust E., Michard R., Nieto J.-L., Poulain P., 1996, A&AS 116, 429
Andreon S., Davoust E., Poulain P., 1997, A&AS 126, 67
Bender R., 1990, A&A 229, 441
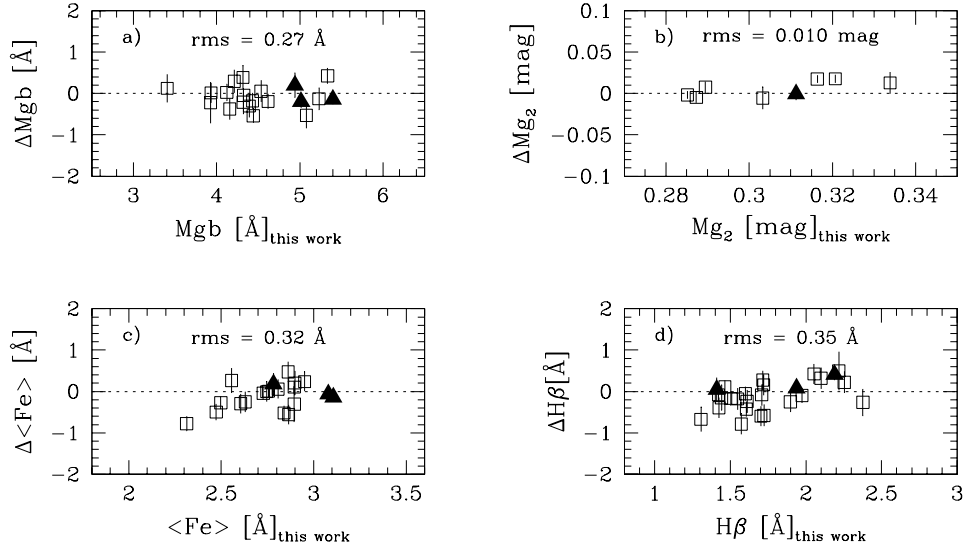Bender R., Möllenhoff C., 1987, A&A 177, 71 (BM87)

Fig. 13. Comparison between the line indices measured from our data and the aperture corrected mean values from J99, within the circular standard aperture having a diameter of $2r_A = 3.4''$. The "slit-equivalent" radius r_L is $1.2''$, $1.7''$ and $2.5''$ for the CA, McD, and MDM setup, respectively (see text). Filled triangles are the cD galaxies. Δ is calculated as "this work" - "literature"

Bender R., Saglia R.P., Gerhard O., 1994, MNRAS 269, 785 (BSG94)

Bertola F., Cinzano P., Corsini E.M., Rix H.-W., Zeilinger W.W., 1995, ApJ 448, L13

Bregman J.N., Hogg D.E., Roberts M.S., 1992, ApJ 387, 484

Burstein D., Heiles C., 1984, ApJS 54, 33

Davies R.L., Illingworth G., 1983, ApJ 266, 516

Davies R.L., Birkinshaw M., 1988, ApJS 68, 409

Davies R.L., Sadler E.M., Peletier R.F., 1993, MNRAS 262, 650 (DSP93)

Dressler A., 1980, ApJS 42, 565 (D80)

Faber S.M., Friel E.D., Burstein D., Gaskell C.M., 1985, ApJS 57, 711

Fernie J.D., 1983, PASP 95, 782

Fisher D., Franx M., Illingworth G.D., 1995, ApJ 448, 119

Fisher D., Illingworth G.D., Franx M., 1995, ApJ 438, 539 (FFI95)

Gerhard O.E., 1993, MNRAS 265, 213

Gerhard O.E., Jeske G., Saglia R.P., Bender R., 1998, MNRAS 295, 197

Godwin J.G., Metcalfe N., Peach J.V., 1983, MNRAS 202, 113 (GMP83)

Gonzales J.J., 1993, Ph.D. Thesis, University of California, Santa Cruz (G93)

Gorgas J., Efstathiou G., Aragon-Salamanca A., 1990, MNRAS 245, 217

Goudfrooij P., Hansen L., Jørgensen H.E., et al., 1994, A&AS 105, 341

Goudfrooij P., Emsellem E., 1996, A&A 306, L45

Holtzman J.A., Burrows C.J., Casertano S., et al., 1995, PASP 107, 1065

Jørgensen I., 1994, PASP 106, 967 (J94)

Jørgensen I., Franx M., 1994, ApJ 433, 553 (JF94)

Jørgensen I., Franx M., Kjærgaard P., 1995a, MNRAS 273, 1097 (JFK95a)

Jørgensen I., Franx M., Kjærgaard P., 1995b, MNRAS 276, 1341 (JFK95b)

Jørgensen I., 1999, MNRAS 306, 607 (J99)

Lucey J.R., Guzmán R., Carter D., Terlevich R.J., 1991, MNRAS 253, 584

Mehlert D., Saglia R.P., Bender R., Wegner G., 1998, A&A 332, 33 (MSBW98)

Peletier R.F., 1989, Ph.D. Thesis, University of Groningen, The Netherlands

Poulain P., Nieto J.-L., 1994, A&AS 103, 573 (PN94)

Rocca-Volmerange B., Guiderdoni B., 1988, A&AS 75, 93

Saglia R.P., Burstein D., Bertschinger G., et al., 1997b, MNRAS 292, 499

Saglia R.P., Bertschinger G., Baggley G., et al., 1997a, ApJS 109, 79

Seaton M.J., 1979, MNRAS 187, 785

van der Marel R.P., Franx M., 1993, ApJ 407, 525

Worthey G., 1992, Ph.D. Thesis, University of California, Lick Observatory

Worthey G., 1994, ApJS 95, 105

Appendix A: Photometric data

Here we present the results of the surface brightness and isophotal shape analysis described in Sect. 2. Tables 5 to 12 are only available in electronic form at the CDS via anonymous ftp to cdsarc.u-strasbg.fr (130.79.128.5) or via http://cdsweb.u-strasbg.fr/Abstract.html and list following parameter of the investigated galaxies:

a: Major axis distance from galaxy center.

b: Minor axis distance from galaxy center.

SB: Local surface brightness along a.

ϵ: Local ellipticity along a.

$\delta\epsilon$: Error of the local ellipticity ϵ.

PA Local position angle (N $\geq$ E) along a.

δ PA: Error of the local position angle PA.

a_i/a: the i-th Fourier coefficients of the cosine function.
b_i/a: the i-th Fourier coefficients of the sine function.
δfc: the error of the Fourier coefficients a_i/a and b_i/a as computed in BM87.

Appendix B: Spectroscopic data

Here we present the spectroscopic results described in Sect. 5. Tables 13 to 82 are only available in electronic form at the CDS via anonymous ftp to cdsarc.u-strasbg.fr (130.79.128.5) or via http://cdsweb.u-strasbg.fr/Abstract.html. Tables 13 to 47 list following kinematical parameter of the investigated galaxies:

r: Major axis distance from galaxy center.
$v(r)$: Line of sight mean velocity.
δv: Error of $v(r)$.
σ: Line of sight velocity dispersion.
$\delta\sigma$: Error of σ.
H_3: Third order coefficient of the Gaussian Hermite decomposition of the line LOSVD.
δH_3: Error of H_3.

H_4: Fourth order coefficient of the Gaussian Hermite decomposition of the line LOSVD.
δH_4: Error of H_4.

Tables 48 to 82 list following line indices of the investigated galaxies:

r: Major axis distance from galaxy center.
$H\beta$: $H\beta$ absorption index.
$\delta H\beta$: Error of $H\beta$.
Mgb: Mgb absorption index.
δMgb: Error of Mgb.
$< Fe >$: $<Fe>$ absorption index.
$\delta < Fe >$: Error of $<Fe>$.
$[MgFe]$: $[MgFe]$ absorption index.
$\delta[MgFe]$: Error of $[MgFe]$.
Mg_2: Mg_2 absorption index (if measured).
δMg_2: Error of Mg_2.
NaD: NaD absorption index (if measured).
δNaD: Error of NaD.

The galaxy number indicated in Tables 1 and 3 as well as in Fig. 6 are given in brackets in the captions.